Journal of Computers Vol. 36 No. 5, October 2025, pp. 445-461
https://doi.org/10.63367/199115992025103605029

Temperature Field Simulation and Intelligent Optimization Method for Preparation Process Parameters of Iron-Based Ceramic Coating ZrO_2-Al_2O_3

Sheng-Wu Kong[1,2*] and Wei-Tao Jia[1]

[1] Hebei Institute of Mechanical and Electrical Technology,
Xingtai City 054000, Hebei Province, China
243047072@qq.com, 1028946189@qq.com

[2] Xingtai Mold Material Technology Innovation Center,
Xingtai City 054000, Hebei Province, China

Received 1 August 2025; Revised 22 September 2025; Accepted 7 October 2025

Abstract. The research on ceramic powders has always been one of the main research directions of laser cladding technology. This article mainly focuses on the numerical simulation method of temperature field and intelligent optimization of preparation parameters in the laser cladding preparation process of iron-based ceramic layers, in order to optimize the overall process of preparing iron-based ceramic coatings. Firstly, the generation and transfer of laser heat, as well as the heat absorption process of materials, were analyzed and constructed. After determining the Gaussian three-dimensional heat source model, the temperature field of the heat source model was simulated using ANSYS software to obtain appropriate laser power and other parameters. Then, based on various process parameters such as coating material, material supply method, pre coating thickness, laser power scanning rate, and spot size during the preparation process, a multivariate non-linear model of processing parameters and various performance measurements was constructed with melting power and feed rate as inputs, dilution rate and overlap rate as responses. Nonlinear regression analysis was then conducted, and an improved differential evolution algorithm was used to solve the optimal solutions of various parameters in the layer preparation process. Finally, simulation experimental results were presented to verify the effectiveness and feasibility of the proposed method in this paper.

Keywords: Laser cladding, numerical simulation, ZrO_2-Al_2O_3, improved differential evolution algorithm

1 Introduction

The material failure caused by the mutual friction between materials is one of the main reasons for the damage and failure of most equipment and parts. Related studies have shown that 80% of mechanical components fail due to wear and tear, and over 50% of mechanical accidents are caused by severe wear and tear of parts. The annual losses caused by friction in the machinery and machinery related industries in the United States account for 4% of the total national economic income, approximately 100 billion US dollars. As a major manufacturing country, China's data on failure losses caused by friction will only become even larger. According to the research conclusion of the China Association for Science and Technology, China suffers economic losses of up to trillions of yuan annually due to friction and wear, especially in industries such as industrial cutting tools, agricultural equipment, mining equipment, and metallurgical manufacturing. The annual losses caused by workpiece wear and failure are about 40 billion yuan. With the emergence of new technologies and products, the annual losses caused by wear and tear are still increasing at a growth rate of 5% to 10%. How to reduce wear and improve the wear resistance of materials is a common concern in the material preparation industry. By coating ceramic materials on the friction surface of metal parts, it is possible to effectively combine the advantages of good toughness and ease of processing of metal materials with the high temperature resistance and oxidation resistance of ceramic powders, and produce products with better performance. Therefore, it is particularly important to coat the surface of mechanical parts with new wear-resistant materials to meet the increasingly high demand for wear resistance [1].

Laser cladding technology is a method of improving the surface properties of materials. It uses a high-energy

* Corresponding Author

density laser beam as a heat source to rapidly melt and solidify the powder pre-set on the substrate surface or the powder sent out through the cladding nozzle with the substrate surface, forming a metallurgical bonding layer with high hardness, good wear resistance, and low dilution rate. This enhances and improves the performance of the parts and extends their working life. Laser cladding technology utilizes carbide ceramic phases to significantly improve surface wear resistance. Based on metallurgical bonding, it ensures a strong bond between the coating and the substrate, effectively enhancing the performance of components under harsh wear conditions. During the cladding process, the instantaneous high temperature of the laser is used to melt the substrate surface and cladding material, forming a structurally stable and high-performance metallurgical coating on the substrate surface. Laser cladding technology has the advantages of high precision, good controllability, minimal thermal impact on the substrate, and low coating dilution rate [2]. The technical principle is shown in Fig. 1.

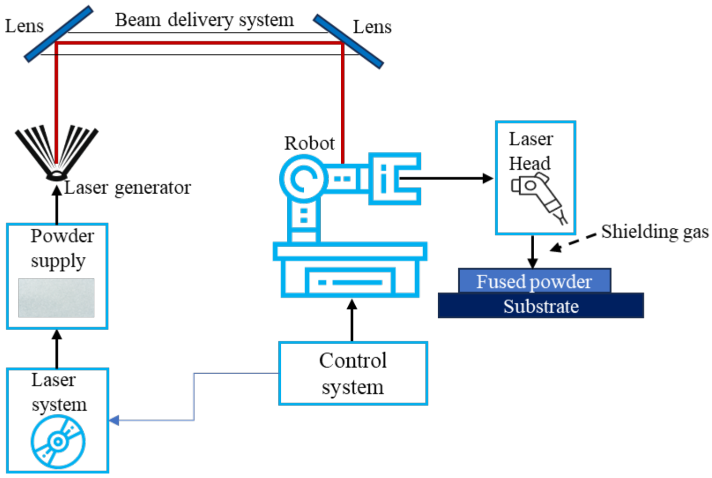

Fig. 1. Principles of Laser cladding process technology

During the cladding process, the molten pool is subjected to laser heat transfer, forming a temperature field. Within this temperature field, the corresponding materials will melt and then form a good metallurgical bond with the substrate. Therefore, the cladding material needs to have excellent wetting and flowability, suitable thermal expansion coefficient, thermal conductivity, melting point, and good deoxidation and slagging ability. As a substrate, iron-based materials have the characteristics of low cost, good surface formability, and excellent processability, and occupy a dominant position in the selection of coating materials.

Ceramic particles and alloys have excellent physical compatibility, with a close metallurgical bond and excellent mechanical properties. Many ceramic metals do not affect the progress of the original metallurgical reaction, and the microstructure of the alloy changes little. Ceramic particles can also be used as nucleating agents for grain refinement [3].

Therefore, the cladding material in this article is iron-based ceramic powder mixed with ZrO_2- Al_2O_3. Both ZrO_2 and Al_2O_3 are high-temperature resistant materials, with Al_2O_3 commonly known as corundum having good wear resistance. ZrO_2 is stable at high temperatures and is not easily corroded or oxidized. Mix these two types of powders thoroughly with the metal cladding powder to complete the temperature field control and preparation parameter optimization in the laser cladding technology process. The work done is as follows:

1) Design experimental powders based on material properties, use ANSYS software to numerically simulate the temperature field of laser cladding, construct heat source models, heat transfer and absorption models, simulate the temperature field, and provide reference for experimental process parameters.

2) Analyze the experimental data, observe its variation patterns, design and use an improved differential evolution algorithm to optimize the experimental data, and extract the optimal preparation parameters. Exploring the changes in Vickers hardness, wear resistance, impact toughness, and other properties of newly formulated powders at the micro level.

3) Complete the experimental design, conduct validation experiments on the methods proposed in this article, and analyze the experimental results.

2 Related Work

This article mainly focuses on the improvement of surface properties of steel, exploring the numerical modeling and simulation of temperature field during the improvement process, as well as the optimization methods of preparation parameters. In related research, Shilu Zhao from Shenyang University used laser cladding technology to prepare TiZrNbV high entropy alloy coating on Q235 steel surface. Under the control of other laser process parameters, the influence of temperature field formed by different laser powers on the surface morphology, microstructure, phase composition, hardness, and friction and wear properties of high entropy alloy coating was studied and compared [4].

Zongjiang Wang applied laser cladding technology to prepare a C22 nickel based alloy cladding layer on the surface of a 45 steel substrate. The results showed that increasing the laser power or decreasing the scanning speed would lead to an overall increase in the width of the cladding layer and the depth of the heat affected zone. The optimal laser cladding process parameters were a scanning speed of 80 mm/s and a laser power of 1750 W. These parameters resulted in the highest height of the single-layer cladding layer and suitable width and depth of the cladding layer and heat affected zone [5].

Guangyao Xie from Soochow University used macro micro modeling and simulation to calculate the temperature field of the molten pool during the hollow ring laser cladding process using ANSYS software. The temperature field results were transformed using a microstructure dynamic growth condition model, and the transformed results were input into a phase field method model of microstructure evolution modeled using MATLAB. The entire study mainly introduced simulation and analysis methods [6].

Xiaoming Xie summarized his research and systematically reviewed the current research status of numerical simulation of multiple physical fields, starting from the dynamic evolution of thermal mechanical flow in the melting process. At the same time, regarding the issue of crack control, summarize the influencing factors that lead to crack formation, and outline the inherent relationship between multi physics field coupling dynamic evolution process optimization crack control. Accurate simulation results are a necessary condition for effectively guiding practice, but current numerical simulation research is still difficult to accurately reflect the actual cladding situation. Finally, point out the difficulties that affect the accuracy of simulation and provide prospects for them [7].

Artificial intelligence neural networks play an important role in optimizing and predicting the parameters of laser cladding preparation processes. Evaluate the influence of process parameters on the geometric morphology and porosity of the cladding layer as optimization objectives. Based on the grey correlation theory, predict the optimal process parameters for the cladding layer and conduct experimental verification. The optimized overlay layer is mainly composed of cellular crystals, and a good metallurgical bond is formed between the overlay layer and the substrate. The Taguchi grey correlation method was used to optimize the laser cladding process parameters, greatly reducing the number of experiments [8].

Yanbin Du, also from Chongqing Technology and Business University, aimed at the influence of process parameters on the dilution rate, aspect ratio, and microhardness of the cladding layer. Taking the laser cladding of 15-5PH powder on the surface of 12Cr13 stainless steel as an example, a fitting regression mathematical model between process parameters and cladding layer quality was constructed. The multi-objective optimization problem was transformed into a single objective problem through the combination of layer analysis method and coefficient of variation method (AHP-CV), and the CWOA algorithm was used to achieve process parameter optimization, which improved the algorithm performance [9].

Junhua Wang from Henan University of Science and Technology used laser power, preheating temperature, and scanning speed as controllable input parameters, and the aspect ratio, saturation, and wetting angle of the cladding layer as outputs. A response value nonlinear mathematical model was constructed using the Macquart algorithm to explore the influence of optimization variables and their weight ranking on the macroscopic morphology of the cladding layer. The second-generation non dominated genetic algorithm was used for optimization, and the Pareto optimal frontier was output to determine the optimal process parameters [10].

Jianghong Lin from Kunming University of Science and Technology designed a four factor four level orthogonal experiment with laser power, scanning speed, powder feed rate, and overlap rate as inputs to optimize the laser cladding repair process parameters of H13 mold steel and obtain a better comprehensive performance cladding layer. H13 powder was deposited on an H13 substrate to prepare a cladding layer. The cladding layer prepared using the process parameters optimized by GRA-EWM method had higher comprehensive performance [11].

In summary, by analyzing and summarizing the relevant research results, many scholars have made relevant achievements in the relevant research fields. In order to demonstrate the relevant research results, this article is divided into the following chapters: Section 2 mainly summarizes and compares the results of simulating the temperature field of laser cladding and optimizing the process parameters in the cladding process. Section 3 completes the construction of the temperature field heat source model distribution, heat source transfer, and heat source absorption models in the laser cladding process. Section 4 mainly completes the functional relationship between experimental factors and response values, establishes a regression surrogate model, and then uses differential optimization algorithm to optimize and solve the parameters. Section 5 describes the process and results of temperature field simulation experiments, as well as the algorithm. The comparative analysis has demonstrated the improved performance of the algorithm, Section 6 is the conclusion section, which summarizes the research findings of this article and explores the shortcomings in the research process, while also planning for further research directions.

3 Modeling and Numerical Simulation of Temperature Field in Laser Cladding

Laser cladding is a tissue regeneration process that involves physical bonding and chemical reactions generated under a laser thermal light source. In the process of metallurgical bonding, the melting and solidification of materials are also accompanied, and thermal energy transfer, material energy absorption, and some motion boundary problems need to be considered. Using experimental methods to melt each prepared powder requires high costs, and considering the small volume of the melt pool, it is difficult to study the temperature distribution and convection of the metal liquid during the melting process. Therefore, in this section, the temperature field of laser cladding is simulated using ANSYS finite element analysis software. The materials involved in the process are high melting point materials such as ZrO_2 and Al_2O_3. Therefore, the optimal laser cladding power is obtained as the final simulation optimization objective. Due to the dynamic nature of the entire cladding simulation process, this paper uses the birth death element technique to simulate the movement of the heat source during the entire cladding process, and then performs solution calculations by discretizing the entire finite body and solving for each discrete individual to integrate the overall results. The process is as follows:

Firstly, the pre modeled substrate entity is imported into ANSYS software and meshed. Then, it is necessary to edit the properties of various materials in the simulation and apply boundary conditions. Further construct the heat source model of the laser in this article, which includes two parts: the laser energy acting on the material and the material's absorption process of the laser: 1) During the laser processing, the laser beam generated by the laser acts on the material after a certain distance of transmission. Due to the different types of beams, different laser energy distributions are generated on the surface of the material; 2) The surface of the irradiated material reflects the laser, with some of the laser energy being reflected back into the surrounding environment and the remaining energy being absorbed by the material; 3) The absorbed laser energy interacts with the material, resulting in different energy distribution states in the interaction area. The mathematical model describing this distribution state is the laser heat source model. 4) The material that interacts with the laser will transfer energy to other parts of the material through thermal conduction, which is the heat transfer process of the material [12].

3.1 Energy Distribution Model of Laser Heat Source

This paper employs a three-dimensional (3D) conical Gaussian heat source model, which is specifically suited for simulating the thermal behavior induced by A-type high-power semiconductor lasers. Unlike traditional surface heat sources, which primarily describe the heat flux distribution in a two-dimensional planar surface, the 3D conical Gaussian heat source is a volumetric representation [13]. It not only describes the thermal energy distribution across the entire surface but also the depth of the heat source's penetration into the material during the melting process. This property makes it particularly suitable for simulating laser-based processes such as welding, cladding, and additive manufacturing, where both surface and subsurface thermal effects play a crucial role. Using a 3D conical Gaussian heat source ensures excellent melt pool symmetry, which is crucial for achieving uniform melting, minimizing defects, and predicting microstructural evolution. Its mathematical formulation captures both the radial and axial decay of the laser intensity, reflecting the physical behavior of laser energy distribution during actual processing. By adjusting heat source parameters such as beam radius, penetration depth, and power density, the model can be customized to more closely resemble experimental conditions. The heat flux density of the 3D conical Gaussian heat source can be written as:

$$q\left(x,y,z,t\right)=\frac{3Q}{pc^2}e^{\left(\frac{-3x^2}{c^2}-\frac{3\left[z+v\left(\tau-t\right)\right]^2}{c^2}\right)} \tag{1}$$

In the formula, $q(x, y, z, t)$ represents the heat flow rate at point (x, y, z) and time t on the fusion surface, Q represents the energy input rate, c represents the concentration coefficient of heat, and τ represents the lag time at the maximum density position of the heat source center. The geometric model is shown in Fig. 2.

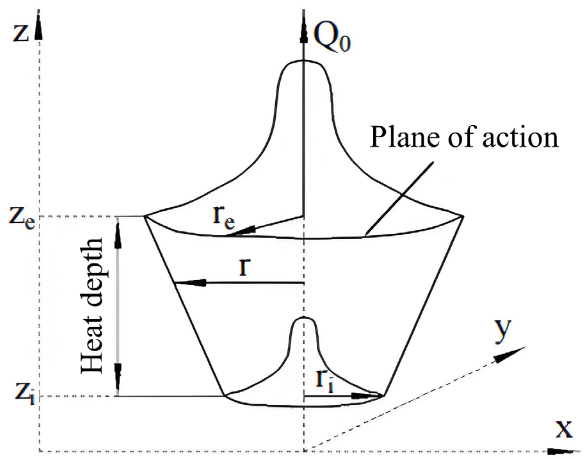

Fig. 2. Schematic diagram of 3D conical Gaussian heat source model

When a laser acts on a material plane, the energy field distribution is proportional to the square of the amplitude of the field distribution. Therefore, the energy distribution of a Gaussian beam acting on a plane perpendicular to the propagation direction is expressed as:

$$E\left(x,y,z\right)=\frac{K}{\omega^2\left(z\right)}\exp\left(-2\frac{x^2+y^2}{\omega^2\left(z\right)}\right) \tag{2}$$

In the formula, K represents a constant factor, and $\omega(z)$ represents the spot radius of the laser beam on the phase plane at point z on the propagation axis. The expression method is:

$$\omega\left(z\right)=\omega_0\sqrt{1+z/f_{laser}} \tag{3}$$

In the equation, f_{laser} represents the focal length parameter of the Gaussian beam.

3.2 The Absorption Model of Laser Energy by Materials

When the laser beam strikes the surface of the cladding material, not all of the incident laser energy participates in the melting process. Instead, it is split into two distinct components: one absorbed by the cladding powder and substrate, and the other reflected or lost to the environment [14]. This energy distribution directly follows the law of conservation of energy, which states that the total input energy must equal the sum of all absorbed and reflected energy. This energy balance can be expressed mathematically as:

$$E_{laser} = E_a + E_r \tag{4}$$

In the equation, E_a represents the energy absorbed by the material, and E_r represents the remaining energy after the laser penetrates the material. As the 3D conical Gaussian heat source used in this article is a three-dimensional heat source, the laser incident depth is relatively large, and the material absorbs the laser through volumetric absorption. According to the Beer Lambert law, when a laser with intensity I_0 is incident on the material, the intensity decreases exponentially with increasing incident depth. The laser intensity at the incident depth h is expressed as:

$$I(h) = I_0 e^{-\lambda h} \tag{5}$$

In the formula, λ represents the absorption coefficient, and the heat source model of the 3D cone Gaussian model is represented as:

$$I(x,y,h) = \frac{2\lambda(1-\eta)P}{\pi(\beta r_0)^2}\exp-\left(\frac{2(x^2+y^2)}{(\beta r_0)^2}+\lambda h\right) \tag{6}$$

In the formula, η represents the reflectivity of the material surface, β represents the Gaussian cone radius correction coefficient, and r_0 represents the Gaussian beam radius.

Considering the reduction of the laser spot radius after the laser is incident on the surface of the material, ignoring the change in the divergence angle of the laser beam transmission process caused by the material, the spot radius at the incident depth h is:

$$r(h) = r_0 + r \cdot \tan\frac{\alpha}{2} \tag{7}$$

In the equation, α represents the angle of Gaussian beam emission.

Therefore, combining equations (1) - (7) yields the final expression for the light source, which takes into account the angle, depth, and time of the light source. Additionally, the expression for a Gaussian light source with a conical shape is shown in equation 8.

$$I(x,y,z,h) = \frac{2\lambda(1-\eta)P}{\pi\beta^2\left[r_0 + r\cdot\tan\alpha/2\right]^2}\exp-2\left(\frac{x^2+y^2}{\beta^2\left[r_0+r\cdot\tan\alpha/2\right]^2}+\lambda h\right) \tag{8}$$

3.3 Simulation Analysis of Heat Source Model

When laser energy strikes the material surface, some of the incident energy is absorbed and redistributed within the substrate and cladding powder through heat conduction. This process controls the heating, melting, and solidification behavior of the cladding layer. This process can be quantitatively described using classical heat conduction principles. According to Fourier's law of heat conduction, the heat flux is proportional to the negative temperature gradient. The three-dimensional transient heat conduction equation can be expressed as:

$$\rho\cdot c\frac{\partial W}{\partial t} = \frac{\partial}{\partial x}\left(k\frac{\partial T}{\partial x}\right)+\frac{\partial}{\partial y}\left(k\frac{\partial T}{\partial y}\right)+\frac{\partial}{\partial z}\left(k\frac{\partial T}{\partial z}\right)+q(x,y,z,h) \tag{9}$$

In the formula, ρ represents the material density, q represents the heat generated by the laser in the material per unit time, k is the thermal conductivity, c is the specific heat capacity of the material, W is the temperature, and t is the time.

Due to various factors such as laser manufacturing errors and optical path transmission, the actual energy distribution of the laser output beam deviates from the ideal energy distribution. To study the influence of different energy distribution heat source models on simulation results, ANSYS was used to conduct finite element modeling and simulation analysis of the heat transfer process of laser fixed-point heating of 45 # steel plate. Due to the fact that the entire single pass cladding process takes 30 seconds, in order to observe the changes in the highest temperature of the laser focus during the cladding process, the time nodes are set as the starting stage of cladding, and 15 seconds and 30 seconds are recorded for simulation.

After the above process, a temperature field simulation model was constructed, and then a laser source model can be established through ANSYS software. By loading different laser powers, different temperature field results can be simulated.

4 Optimization of Process Parameters in Laser Cladding Process

Laser cladding technology is a metallurgical process related to many aspects such as physics, chemistry, and materials science. There are many factors that affect the quality of the cladding layer, including cladding materials, material supply methods, pre coating thickness, laser power scanning rate, spot size, and other factors that affect each other. This article analyzes the impact of laser processing technology on the quality of the cladding layer from the perspectives of cladding power, feed rate, dilution rate, and overlap rate.

Establish a multivariate nonlinear model by comparing the processing parameters of all cladding layers with the measured values of various properties, and conduct nonlinear regression analysis. Using the processing parameters of all cladding layers as input layers and performance measurements as output layers, establish an improved differential evolution algorithm model and analyze its training process and accuracy. Through simple differential mutation operations and one-on-one competitive survival strategies, the population's mutation process is continuously executed to ultimately solve for the optimal value [15].

4.1 Fitting Regression Analysis

In this section, the team utilize Minitab's regression analysis capabilities to construct a surrogate model to capture the functional relationship between experimental factors and their corresponding response values [16]. In this context, the primary purpose of using regression is to approximate the complex, nonlinear mapping between process parameters and performance metrics using a mathematically tractable model that is easy to analyze, interpret, and apply for optimization. By fitting experimental data using Minitab's regression module, the variability of the response can be decomposed into the contributions of individual factors, their interactions, and higher-order terms. To this end, the team construct a regression surrogate model in which the true, but unknown, functional relationship between the independent variables and the dependent response is replaced by an approximate function based on experimental observations. Minitab provides statistical tools such as analysis of variance (ANOVA), p-values, and R^2 metrics to assess the significance of each factor and the overall quality of the model fit, ensuring that the surrogate model has both predictive accuracy and statistical validity. A high-order polynomial regression model was chosen as the surrogate model for this study because its flexible polynomial form can represent both linear and nonlinear trends. The general form of a high-order polynomial regression surrogate model can be expressed as:

$$y = a_0 + a_1 x_1 + a_2 x_2 + a_{11} x_1^2 + a_{22} x_2^2 + a_{12} x_1 x_2 + \varepsilon \tag{10}$$

In the equation, x_i is the input a_1, a_2, a_{11}, a_{22}, a_{12} are partial regression constants, where a_1 and a_2 are coefficients related to the main parameters, a_{11} and a_{22} are quadratic coefficients, and a_{12} is the interaction coefficient.

Considering the different emphasis on each sub target in the laser cladding process, the Analytic Hierarchy Process is introduced. The weight values of the dilution rate and overlap rate of the cladding layer response are calculated as follows:

$$\begin{cases} t_{ij} = \dfrac{\omega_{ij}}{\sum_{i=1}^{n} \omega_{ij}} \\ \omega_i = \sum_{j=1}^{n} m_{ij} \\ \hat{\omega}_i = \dfrac{\omega_i}{\sum_{i=1}^{n} \omega_i} \end{cases} \tag{11}$$

Dilution rate is a measure of the degree to which elements in the cladding layer are diluted due to the mixing of matrix material elements into the cladding layer. In this article, the dilution rate is expressed using the height of the cladding layer, $\eta_{Di-rate}$ represents dilution rate, h_{base} represents substrate height, and $h_{clad-layer}$ represents cladding layer height.

$$\eta_{Di-rate} = \frac{h_{base}}{h_{clad-layer} + h_{base}} \tag{12}$$

Construct model formulas for laser cladding power, feed rate, dilution rate, and overlap rate in the model.

$$E = \frac{P}{D} \cdot V_b \tag{13}$$

In the formula, P is the laser beam power, D is the laser beam spot diameter, and V_b represents the laser scanning speed. The laser energy density E is an important parameter that reflects the laser power. If E is too high, the energy obtained by the melt pool will be too high, the dilution rate will increase, and even overheating will occur. The surface of the cladding layer will be uneven. If E is too low, the energy obtained by the melt pool will be too low, and the depth of substrate melting will be too low, resulting in the detachment of the cladding layer or insufficient melting of the cladding material. The surface of the cladding layer will produce nodules or holes, which seriously affects the quality of the cladding layer. To quantitatively analyze the influence of process parameters on the cladding quality, the relationship between the response variable and input parameters can be formulated as:

$$Q = f(P, d, v, f). \tag{14}$$

Here, f represents the physical mapping from process parameters to the resulting quality metrics. The optimization problem for finding the best parameter set can then be expressed as:

$$\min_{P,d,v,f} L(Q(P, d, v, f)) \tag{15}$$

Without changing other parameters, excessive feed rate can easily lead to insufficient melting of the melted powder, the formation of lumps, and even direct detachment of the melted layer; A too low feed rate can cause overburning, and even deformation of the substrate, ultimately leading to cracks in the cladding layer.

The input parameters and response values discussed in this article are relatively few, but according to their mutual influence relationship, there is an optimal result between each parameter and response value. If the optimal result is found by empirical or experimental methods, it undoubtedly increases the economic and time costs of the experiment. At the same time, the optimal parameters and response values are a certain numerical point, which cannot be accurately found by experimental methods. Therefore, this article introduces intelligent algorithms to solve for the optimal parameters.

4.2 Using Improved Differential Evolution Algorithm to Solve Optimal Parameters

The basic principle of this algorithm is to mimic the evolutionary development of natural biological populations and adhere to Darwin's philosophy of "survival of the fittest." The algorithm first uses real-number encoding to represent candidate solutions, allowing each individual in the population to directly correspond to a continuous variable vector in the solution space. This representation is particularly effective for optimization problems that require precise and flexible handling of continuous parameters. After the population is initialized, the algorithm evolves through a series of operations. The key operation is a mutation mechanism based on individual differences. Specifically, for each target vector in the population, a mutation vector is generated by adding the weighted difference of two randomly selected population vectors to a third vector. This differential mutation strategy introduces diversity and effectively explores the search space by guiding new candidate solutions toward promising regions [17]. Mutation is typically followed by a crossover operation, combining the elements of the mutation vector with those of the target vector to generate a trial vector [18]. This process ensures a balance between exploration and exploitation. The final step of each iteration is a one-to-one survival strategy, which embodies the principles of natural selection. A test vector competes directly with its corresponding target vector: if the test vector's fitness value is superior, it replaces the target vector in the next generation; otherwise, the original target vector is retained. This mechanism ensures that the population steadily evolves towards higher fitness over generations. By repeatedly applying mutation, crossover, and selection, the algorithm gradually improves the overall quality of the population, eventually converging to an optimal or near-optimal solution. The process can be summarized as follows:

1) Group initialization, randomly generating an initial population of size N in the n-dimensional solution space of the multi pass overlapping laser cladding fitting regression model:

$$Q(0)=\left[Q_1(0),Q_2(0),\cdots,Q_N(0)\right] \tag{16}$$

The dimension of chromosomes in an individual is represented as follows:

$$q_{ij}(0)=q_{ij,\min}+\left(q_{ij,\max}-q_{ij,\min}\right)\cdot\delta \tag{17}$$

$q_{ij,\max}$ and $q_{ij,\min}$ represent the upper and lower bounds of chromosomes, while C represents a random distribution between 0-1.

2) Mutation, performing mutation operations on individual $Q_i(t)$ in a certain generation population to obtain new mutated individuals, the mutation operations are as follows:

$$V_i(t+1)=Q_{i1}(t)+BY\left(Q_{i2}(t)-Q_{i3}(t)\right) \tag{18}$$

$Q_{i1}(t)$ is the parent base vector, $Q_{i2}(t) - Q_{i3}(t)$ is the parent differential vector, which is the key to differential evolution algorithm, and BY is the mutation factor.

3) Crossover, to increase the diversity of the population, crossover operations are performed on the obtained mutant individuals;

$$u_{ij}(t+1)=\begin{cases}V_{ij}(t+1) & \tau\le JX\\ q_{ij}(t) & \tau>JX\end{cases} \tag{19}$$

In the formula, u represents the selected individual, JX represents the crossover factor, and τ is a random number that follows a uniform distribution.

4) Select and compare the fitness values of the selected individual and the current individual based on the corresponding values of laser cladding. Repeat step 2 until the optimal solution is reached, which is represented as follows:

$$Q_i(t+1)=\begin{cases}U_i(t+1) & f(U_i(t+1))\geq f(Q_i(t))\\ Q_i(t) & f(U_i(t+1))<f(Q_i(t))\end{cases} \quad (20)$$

5) Improvement: In the mutation stage, an adaptive scaling factor is used instead of a fixed mutation factor. The adaptive scaling factor can be adjusted with the number of iterations, thus solving the problem of insufficient search ability caused by fixed factors.

$$S(t)=S_{\min}+(S_{\max}-S_{\min})\frac{S_{p1}(t)-S_{p2}(t)}{S_{p1}(t)-S_{p3}(t)} \quad (21)$$

$S_{\max}$ and $S_{\min}$ are the upper and lower limits of the scaling factor, respectively. The initial chaotic factor sequence is generated using the commonly used one-dimensional mapping method for chaotic systems, and the basic expression is as follows:

$$s_{factor}(t)=\xi\cdot s_{factor}(t-1)\left[1-s_{factor}(t-1)\right] \quad (22)$$

In the formula, $s_{factor}(t)$ represents the chaotic search factor, with a value between 0 and 1, and ξ determines the chaotic state of the entire system, the algorithm flowchart is shown in Fig. 3.

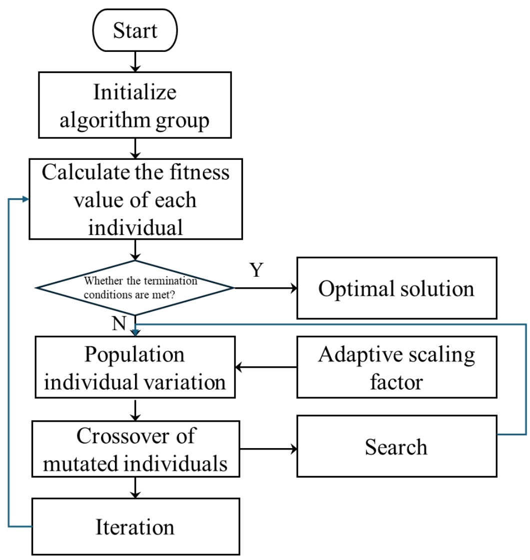

Fig. 3. Algorithm flowchart

The algorithm pseudocode is as follows:

```
// Initialize the population P_0 using chaotic sequences for better uniformity
for i = 1 to NP do
    for j = 1 to D do
        // Generate a chaotic number in [0, 1] and map it to the variable’s domain
[L_j, U_j]
        chaos_value = Chaotic_Map(initial_seed)
        X_{i, 0}^j = L_j + chaos_value * (U_j - L_j)
        initial_seed = chaos_value // Update the seed for the next value
    end for
    // Evaluate the fitness of the initial individual
```

```
        f(X_{i, 0}) = evaluate(X_{i, 0})
    end for
    X_best = individual with the best fitness in P_0
    f_best = f(X_best)
    G = 1
    while (G <= G_max) and (stopping criterion not met) do
        // Strategy 1: Generation-based adaptive parameters (common approach)
        F = F_upper - (F_upper - F_lower) * (G / G_max) // Linearly decrease F
        CR = CR_lower + (CR_upper - CR_lower) * (G / G_max) // Linearly increase CR
         // Strategy 2: Individual-based adaptive parameters using chaos (more ad-
vanced)
        // for i=1 to NP do
        //   F_i = F_lower + Chaotic_Map() * (F_upper - F_lower)
        //   CR_i = CR_lower + Chaotic_Map() * (CR_upper - CR_lower)
        // end for
        for i = 1 to NP do
           do
                r1 = floor(Chaotic_Map() * NP) + 1
            while (r1 == i)
            do
                r2 = floor(Chaotic_Map() * NP) + 1
            while (r2 == i or r2 == r1)
            do
                r3 = floor(Chaotic_Map() * NP) + 1
            while (r3 == i or r3 == r1 or r3 == r2)
            V_i = X_{r1, G-1} + F * (X_{r2, G-1} - X_{r3, G-1})
            for j = 1 to D do
                if V_i^j < L_j then
                    V_i^j = L_j
                else if V_i^j > U_j then
                    V_i^j = U_j
                end if
            end for
            j_rand = floor(Chaotic_Map() * D) + 1
            // Initialize the trial vector U_i
            for j = 1 to D do
                // Use chaotic value to decide if crossover should happen
                if (Chaotic_Map() <= CR) or (j == j_rand) then
                    U_i^j = V_i^j // Inherit from mutant vector
                else
                    U_i^j = X_{i, G-1}^j // Inherit from target vector
                end if
            end for
            f_trial = evaluate(U_i) // Evaluate the fitness of the trial vector
            if f_trial <= f(X_{i, G-1}) then
                // If the trial vector is better or equal, it survives
                X_{i, G} = U_i
                f(X_{i, G}) = f_trial
                // Check if this is the new global best solution
                if f_trial < f_best then
                    X_best = U_i
                    f_best = f_trial
                end if
            else
                // If not, the target vector is carried over to the next generation
                X_{i, G} = X_{i, G-1}
                f(X_{i, G}) = f(X_{i, G-1})
            end if
        G = G + 1 // Proceed to the next generation
        // Optional: Record statistics (e.g., best fitness per generation)
    end while // End of evolutionary loop
    Output the best found solution: X_best and its fitness f_best
```

5 Simulation Experiment and Result Analysis

5.1 Temperature Field Simulation Results

Fig. 4 shows the peak temperature plots and isotherms at the end of the dwell period for three laser powers. As expected, the temperature field is axisymmetric with a steep vertical gradient due to Gaussian heating, conduction losses in the substrate, and surface convection/radiation. Increasing power increases the peak temperature, widens the melt pool width and depth, and thickens the heat-affected zone (HAZ) [19]. Because losses increase with temperature, the melt pool size increases sublinearly with power.

3000 W. The peak surface temperature approaches the melting range of the Al_2O_3 powder, forming a shallow, lenticular melt pool. The melt zone remains confined near the surface, with limited penetration into the substrate. The isotherms are closely aligned below the laser spot, indicating high local gradients and a relatively small HAZ. This facilitates dimensional control but also narrows the processing window.

3200 W. Additional power increases superheat and extends the melt pool laterally and downward. The solidus-liquidus isotherms shift outward, and the melt pool depth increases significantly. The thermal gradient remains significant, but slightly smaller than at 3000 W, which means slightly slower cooling during shutdown and potentially improved melt trajectory continuity.

3400 W. Further increasing the power results in a wider melt pool and deeper penetration into the substrate. The HAZ expands, and the high-temperature isotherm occupies a larger area. While this behavior improves wettability and reduces the risk of incomplete fusion, it also increases the risk of excessive remelting of the underlying layer and generates higher residual thermal stresses during cooling. For ceramics like Al_2O_3, care must be taken to avoid thermal shock-induced cracking as the gradient increases.

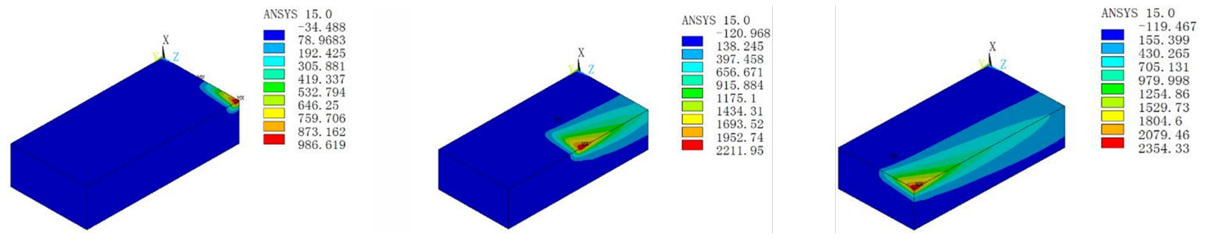

a) Temperature Field Simulation at 3000W Power

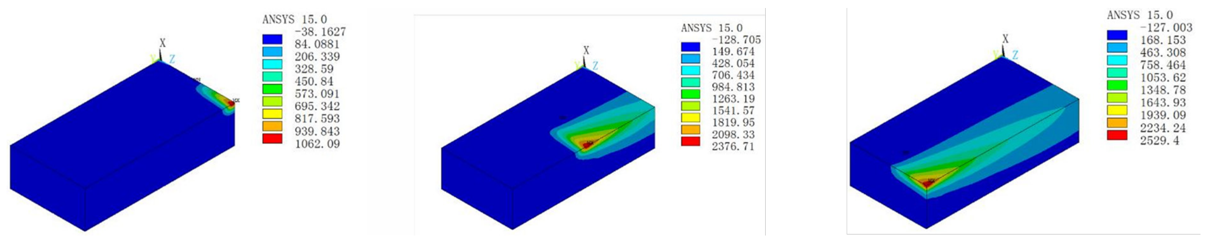

b) Temperature Field Simulation at 3200W Power

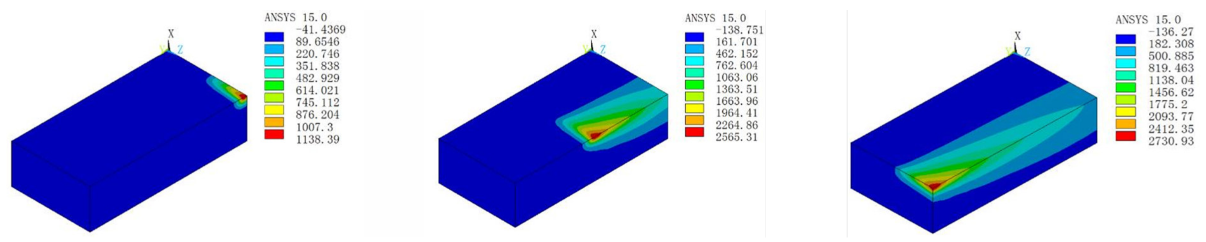

c) Temperature Field Simulation at 3400W Power

Fig. 4. Temperature field simulation at different powers and times

From Fig. 4, it can be seen that the entire single pass cladding process takes 30 seconds. In order to observe the change in the highest temperature of the laser focus during the cladding process, the time nodes are set as the beginning stage of cladding, and 15 seconds and 30 seconds are recorded as three points for simulation. When the power is 3000W, the highest temperature reached the melting point of the powder Al_2O_3 used during the melting process, but did not reach the melting point of ZrO_2 at 2677 ℃. When the power is 3200W, it is also impossible to reach the melting points of the two powders. When the power is at 3400W, the temperature at the laser focal length during the cladding process is very high, reaching a maximum of 2730 ℃, which is the melting point of ZrO_2. Therefore, the guidance power for the cladding experiment is 3400W. The simulation results show that the temperature increases continuously from the initial stage, to the middle stage, and finally to the end, until the expected temperature is reached. Therefore, it is recommended to preheat the unprinted sheet before the melting experiment begins, so that the experiment can reach a higher temperature from the beginning and reduce experimental errors. When the power is at 3400W, the material temperature rapidly drops to 500 ℃ within 20 seconds after the completion of cladding. At 5000s, the temperature of the specimen has already dropped to 22 ℃, which can be used for rough and fine machining of the specimen; Until 8000s, the temperature of the specimen cooled to room temperature of 20 ℃. The cooling process is shown in Fig. 5.

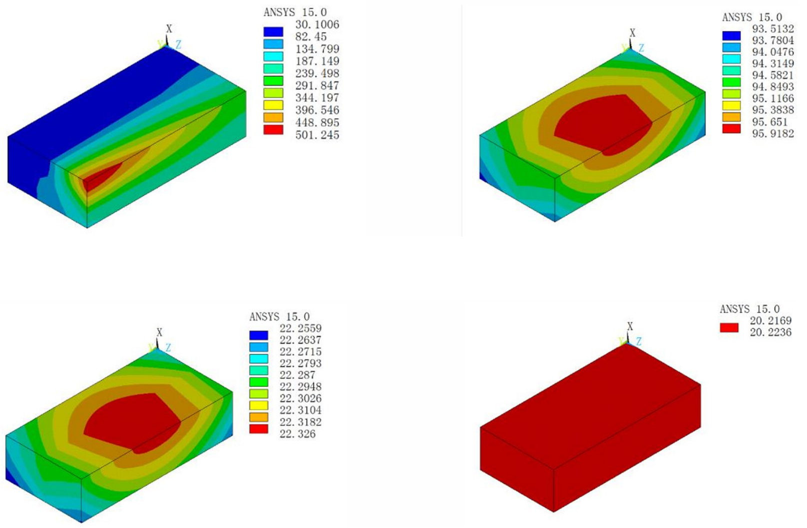

Fig. 5. Simulation of material cooling process

5.2 Optimal Parameter Solution and Result Analysis

To illustrate the improvement in search ability between the improved differential evolution algorithm and the original differential algorithm in this article, a comparison will be made between the two. For fairness, the population size will be taken as 40 and the iteration number T will be taken as 300. The weight values decrease linearly, with an acceleration coefficient of 1.8, a variation factor BY is 0.5, and a minimum scaling factor of 0.2. The fitness curves of the two are shown in Fig. 6.

As shown in Fig. 6, the improved algorithm proposed in this paper has a faster convergence speed, and through the improved search strategy, it can escape from the local optimal region, allowing the population to continue searching for the global optimal solution. Therefore, this algorithm has good robustness for optimizing the parameters of multi pass overlap laser cladding process.

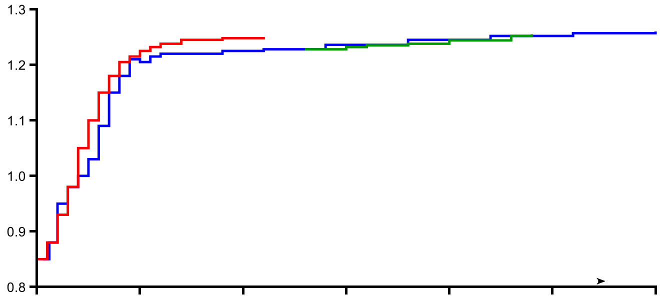

Fig. 6. Comparison of fitness curves between the two

5.3 Determination of Optimal Process Parameters

Using different laser powers for laser cladding of different materials to achieve an appropriate dilution rate in the melt pool is a crucial step in the laser cladding process [20]. This experiment will deposit iron-based alloy on the surface of 45 steel and analyze the effect of different powers on the macroscopic quality of the deposited layer. The powder used is F90-3 powder, because the content of ZrO_2 in this powder is the highest, and ZrO_2 has the highest melting point among all powder components. If ZrO_2 can melt, then other components can reach their melting points. The laser power is selected as 3.4kw, the feed rate was calculated to be 6mm/s, and the experimental equipment is a 4kw high-power semiconductor laser with a focal length of 300mm. The prefabricated powder laying method is used, and the powder laying thickness of 2mm can achieve the optimal process parameters. The actual effect is shown in Fig. 7.

Fig. 7. Experimental results display of fusion effect

F90-3 iron-based powder was used with a power of 3.4 kw. The method of pre-laying powder was used to lay 2mm powder, and the feed rate was calculated to be 4 mm/s. Under this parameter, the melting effect is shown in Fig. 8.

Fig. 8. Display of different parameter results

As shown in the above figure, large-area laser cladding requires low surface roughness, good metallurgical bonding, and a dense, smooth, and crack free surface. The overlap rate has a significant impact on the flatness and surface roughness of the cladding layer. Many scholars have shown that a overlap rate of around 50% yields the best surface quality for cladding. Based on practical experience, the overlap rate for this experiment is set at 50%. The ideal state is to control the dilution rate below 10%, which cannot be too low. An accuracy of around 5% is more appropriate.

5.4 Comparative Analysis of Simulation and Experimental Results

To further validate the rationality and effectiveness of the simulation results, the numerical simulation results were compared with actual experimental results. From a simulation perspective, the use of a three-dimensional conical Gaussian heat source in ANSYS allows for a detailed description of the temperature distribution, melt pool evolution, and subsequent cooling process at different laser powers [21]. As shown in Fig. 9, The simulation results demonstrate that a laser power of 3400 W is sufficient to melt ZrO_2, which has the highest melting point, thereby ensuring that other alloying elements in the F90-3 iron-based powder also reach their melting points. Furthermore, the simulation accurately predicts the rapid temperature drop after cladding, with the specimen cooling to 22°C in approximately 5000 s, consistent with actual processing requirements. From an experimental perspective, under the same process parameters, the cladding layer exhibits low surface roughness, good metallurgical bonding, and a dense, crack-free surface. This validates the feasibility of the simulation method and demonstrates that the optimized parameters can achieve high-quality cladding results. In addition, both simulation and experimental results emphasize the importance of preheating the substrate, which can reduce thermal gradients, minimize residual stresses, and improve melt pool stability. The comparative results also reveal some subtle differences. In the simulation, the temperature distribution appears smoother due to the use of an idealized heat source model. However, in actual applications, the melt pool shape and surface roughness will be affected by external interference such as powder feeding uniformity, shielding gas flow rate, and laser power fluctuations. Despite this, the overall trends of simulation and experiment are highly consistent, indicating that the improved differential evolution algorithm combined with the three-dimensional conical Gaussian heat source model can effectively guide process parameter optimization. This strongly proves that simulation-driven parameter design can shorten the experimental cycle, reduce trial and error costs, and accelerate the application of laser cladding technology in industrial environments.

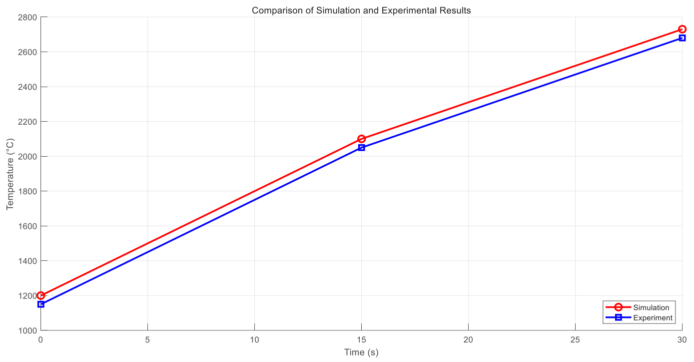

Fig. 9. Comparison between simulation and experimental results of molten pool temperature evolution

6 Conclusion

This article is based on the use of high hardness iron-based powder, and improves it with high-temperature resistant ceramic powders Al_2O_3 and ZrO_2. Five different powders are prepared for melting experiments. And study its microstructure and mechanical properties through experiments. The main research results are as follows:

(1) A numerical analysis model for laser cladding was established using ANSYS finite element analysis software, and the laser cladding process was simulated and analyzed. Based on the high temperature resistance of Al_2O_3 and ZrO_2 ceramic powders, the power in the cladding parameters was adjusted to explore the optimal experimental power. The simulation results show that the suitable melting power for this powder is 3400w. It was found that the heat source during the melting process has a heating process. In order to reduce experimental errors, the specimens need to be preheated in subsequent experiments.

(2) Based on the characteristics of the cladding material, an optimal algorithm for solving process parameters was designed, and feasibility experiments for cladding were conducted. Based on the analysis of the impact of cladding process parameters on cladding quality, the optimal cladding process parameters were determined.

(3) An improved differential evolution algorithm was used. Firstly, a differential evolution algorithm model was constructed, and then an adaptive factor was added to the differential evolution algorithm model to improve the search accuracy of the algorithm and avoid getting stuck in local optima.

The iron-based ZrO_2-Al_2O_3 coating was successfully deposited using laser cladding, and the properties of different material coatings were compared and analyzed, achieving phased results. However, due to limitations in level and time, there are still many issues that need to be studied in the future of this project, mainly in the following two aspects:

1) During the powder melting process, there is a phenomenon of explosion, and powder will escape during the explosion process. Subsequent improvements can be made by improving the powder preparation process and melting process.

2) Due to the fact that ZrO_2 and Al_2O_3 are both high-temperature resistant ceramics, future research can focus on their friction and wear properties at high temperatures, as well as high-temperature creep properties.

7 Acknowledgement

Research on Optimization Design and Manufacturing Technology of Injection Mold Based on UAV Coverage Parts (2024ZC041).

References

[1] Y.-C. Zhang, H.-J. Wang, W.-G. Chen, Research on Friction Resistance Reduction Characteristics of Surface Laser Cladding Modification Technology, Construction Machinery and Equipment 55(9)(2024) 143-146+15.

[2] G.-C. Zhang, J. Lv, B.-Q. Song, X.-H. Men, X.-L. Fu, Research progress on hardness strengthening of laser cladding coating, Manufacturing Technology & Machine Tool (12)(2023) 65-72.
https://doi.org/10.19287/j.mtmt.1005-2402.2023.12.008

[3] W.-N. Wu, W.-L. Sun, J. Lu, J.-T. Yu, Research Progress of Laser Cladding Ceramic Particle Reinforced High Entropy Alloy Coating, Applied Laser 44(5)(2024) 38-48.
https://doi.org/10.14128/j.cnki.al.20244405.038

[4] S.-L. Zhao, J.-C. Wu, G.-F. Ma, L.-Y. Gao, Technology and Properties of Laser Cladding TiZrNbV High-Entropy Alloy Coating on Q235 Steel, Journal of Shenyang University (Natural Science) 36(6)(2024) 464-468+546.
https://d.wanfangdata.com.cn/periodical/shenydxxb202406002

[5] Z.-J. Wang, R.-X. Xie, J. Liao, Preparation and Properties of C22 Nickel-Based Alloy Laser Cladding Coating on 45 Steel Surface, Materials for Mechanical Engineering 48(6)(2024) 67-74.
https://doi.org/10.11973/jxgccl220695

[6] G.-Y. Xie, L.-F. Wang, J.-Q. Luo, G.-X. Zhu, Simulation of Micro-Structure of Molten Pool During Hollow Ring Laser Cladding by Phase Field Method, Applied Laser 44(11)(2024) 12-23.
https://doi.org/10.14128/j.cnki.al.20244411.012

[7] X.-M. Xie, X.-B. Liu, T. Chen, Z.-Y. Liu, Y. Meng, S.-H. Zhang, Research Progress in Numerical Simulation of Laser Cladding Process and Crack Regulation, China Surface Engineering 37(5)(2024) 177-194.
https://doi.org/10.11933/j.issn.1007-9289.20231103003

[8] X.-Y. Yao, Q. Lin, H.-H. Ding, W.-J. Wang, J. Guo, Y. Zhu, L. Gan, Optimization of Process Parameters of Ni60+WC Laser Cladding Coating Based on Taguchi-Grey Relation Method, Surface Technology 52(11)(2023) 394-405+465.
https://doi.org/10.16490/j.cnki.issn.1001-3660.2023.11.034

[9] Y.-B. Du, G.-H. He, Z.-J. Zhou, L.-S. Shu, Microstructure and Properties of 15-5PH Coating by Laser Cladding on 20Cr13 Surface, Laser & Optoelectronics Progress 60(9)(2023) 0914002.
https://doi.org/10.3788/LOP220854

[10] J.-H. Wang, X.-Y. Liang, Y. Lu, J.-F. Xu, J.-J. Peng, Y.-W. Xu, T.-C. Xie, Optimization of broadband laser cladding process parameters based on NSGA-II algorithm, Laser Journal 45(7)(2024) 220-226.
https://doi.org/10.14016/j.cnki.jgzz.2024.07.220

[11] J.-H. Lin, M.-H. Du, C.-Z. Pan, Parameters Optimization of Laser Cladding Process for H13 Mold Steel Surface Based on Comprehensive Statistical Analysis Method, Chinese Journal of Lasers 52(8)(2025) 0802201.
https://doi.org/10.3788/CJL241252

[12] G.-W. Wang, Y. Ding, Y.-C. Guan, Y. Wang, L.-J. Yang, Model Heat Source Using Actual Distribution of Laser Power Density for Simulation of Laser Processing, Journal of Central South University 29(10)(2022) 3277-3293.
https://doi.org/10.1007/s11771-022-5133-3

[13] Z.-D. Zhang, Y.-Z. Huang, A.R. Kasinathan, S.I. Shahabad, U. Ali, Y. Mahmoodkhani, E. Toyserkani, 3-Dimensional heat transfer modeling for laser powder-bed fusion additive manufacturing with volumetric heat sources based on varied thermal conductivity and absorptivity, Optics & Laser Technology 109(2019) 297-312.
https://doi.org/10.1016/j.optlastec.2018.08.012

[14] F. Wirth, D. Eisenbarth, K. Wegener, Absorptivity measurements and heat source modeling to simulate laser cladding, Physics Procedia 83(2016) 1424-1434.
https://doi.org/10.1016/j.phpro.2016.08.148

[15] Y.-B. Du, Z.-J. Zhou, L. Xu, Y. F. Hu, L.-S. Shu, Laser cladding process parameter optimization method based on grey relational analysis and ACDE algorithm, Computer Integrated Manufacturing Systems 28(1)(2022) 149-160.
https://doi.org/10.13196/j.cims.2022.01.015

[16] R. Alizadeh, J.K. Allen, F. Mistree, Managing computational complexity using surrogate models: a critical review, Research in Engineering Design 31(3)(2020) 275-298.
https://doi.org/10.1007/s00163-020-00336-7

[17] A.W. Mohamed, A.K. Mohamed, Adaptive guided differential evolution algorithm with novel mutation for numerical optimization, International Journal of Machine Learning and Cybernetics 10(2)(2019) 253-277.
https://doi.org/10.1007/s13042-017-0711-7

[18] M.-M. Ali, Differential evolution with preferential crossover, European Journal of Operational Research 181(3)(2007) 1137-1147.
https://doi.org/10.1016/j.ejor.2005.06.077

[19] C.W. Buckley, T.L. Bergman, An experimental investigation of heat affected zone formation and morphology development during laser processing of metal powder mixtures, Journal of Heat Transfer 123(3)(2001) 586-592.
https://doi.org/10.1115/1.1370508

[20] A.-F.-H. Kaplan, G. Groboth, Process analysis of laser beam cladding, Journal of Manufacturing Science and Engineering 123(4)(2001) 609-614.
https://doi.org/10.1115/1.1344899

[21] J. Romano, L. Ladani, M. Sadowski, Thermal modeling of laser based additive manufacturing processes within common materials, Procedia Manufacturing 1(2015) 238-250.
https://doi.org/10.1016/j.promfg.2015.09.012